M. Benítez, A. Bermúdez, A second order characteristics finite element scheme for natural convection problems, J. Comput. Appl. Math. 235 (11) (2011) 3270–3284.

A second order characteristics finite element scheme for natural convection problems

M. Benítez[a,*], A. Bermúdez[a]

[a] *Departamento de Matemática Aplicada, Universidad de Santiago de Compostela, Campus Sur s/n, E-15782 Santiago de Compostela, Spain*

Abstract

In this paper a second order characteristics finite element scheme is applied to the numerical solution of natural convection problems. Firstly, after recalling the mathematical model, a second order time discretization of the material time derivative is introduced. Next, fully discretized schemes are proposed by using finite element methods. Numerical results for the two-dimensional problem of buoyancy-driven flow in a square cavity with differentially heated side walls are given and compared with a reference solution.

Key words: natural convection, finite elements methods, characteristics method, Lagrange-Galerkin methods

1. Introduction

Natural convection is present in many real situations, such as room ventilation, double glass window design, etc. More important, it is behind the ocean and atmosphere dynamics. Typically, fluid flow and heat transfer are governed by the partial differential equation system of mass, momentum and energy conservation but in the case of natural convection the so-called Boussinesq approximation is generally employed.

This paper concerns the numerical solution of this problem. Due to the importance of the convective terms and in order to get upwind schemes, we use methods of characteristics in combination with finite elements. These methods are based on time discretizations of the material time derivative and were introduced in the beginning of the eighties of the last century. They have been combined with different space discretizations, for example, finite differences [16], finite elements ([24], [6], [8], [22], [30], [29], [25]), spectral finite elements ([31], [1]), discontinuous finite elements ([3], [2], [4]), and so on. When combined with finite elements they are also called Lagrange-Galekin methods.

Numerical solution of convection-diffusion partial differential equations by this kind of methods is addressed in ([16], [24], [30], [15], [5]) among others. Unconditional stability, independent of the diffusion coefficient, has been obtained in these works. Moreover, in [24] and [30], error estimates are stated. More precisely, if $\triangle t$ denotes the time step, h the mesh-size and k the degree of the finite elements space, estimates of the form

*Supported by the Ministerio de Educación, Cultura y Deporte (Spain).

Email addresses: marta.benitez@usc.es (M. Benítez), alfredo.bermudez@usc.es (A. Bermúdez)

January 13, 2011

$O(h^k) + O(\triangle t)$ in $l^\infty(L^2(\mathbb{R}^m))$-norm are shown in [30] (m denotes the dimension of the spatial domain). In [24] error estimates of the form $O(h^k) + O(\triangle t) + O(h^{k+1}/\triangle t)$ in $l^\infty(L^2(\Omega))$-norm are obtained under the assumption that the normal velocity component vanishes on the boundary of Ω. All of these estimates involve constants which depend on solution norms. For linear finite elements and for a velocity field vanishing on the boundary a convergence of order $O(h^2) + O(\min(h, h^2/\triangle t) + O(\triangle t)$ in $l^\infty(L^2(\Omega))$-norm is stated in [5], where the constants only depend on the data. In principle, the method has been introduced for evolution equations but an adaption to solve convection-diffusion stationary problems has been proposed in [7].

In [27] a second order characteristics method for solving constant coefficient convection-diffusion equations with Dirichlet boundary conditions is studied. The Crank-Nicholson discretization has been used to approximate the material time derivative. For a divergence-free velocity field vanishing on the boundary and a smooth enough solution, stability and $O(\triangle t^2) + O(h^k)$ error estimates in $l^\infty(L^2(\Omega))$-norm are stated (see also [10] and [11] for further analysis).

In this work we use a three points second order formula to discretize the material time derivative. This method has been proposed and analyzed for one-dimensional convection-diffusion equations in [17], and for the incompressible Navier-Stokes equations in [12]. We combine this time discretization with P_1-bubble finite elements for the motion equation and P_2 finite elements for the energy equation.

In order to test the proposed methods, the problem of a buoyancy-flow in a square cavity with vertical sides which are differentially heated is solved for $10^3 \leq Ra \leq 10^7$. This problem is suitable for testing and validating computer codes for convective thermal problems, as the numerous references in the literature show. For example, in [13] numerical solutions to the transient Navier-Stokes equations have been given for laminar convective motion of a gas in an enclosed vertical slot with large horizontal temperature differences. De Vahl Davis [14] uses a finite difference method for solving the stream function-vorticity formulation of the problem; forward differences were used for the time derivatives and second-order central differences for all space derivatives. He describes a benchmark numerical solution obtained by Richardson's extrapolation. It is used in the present paper to assess the proposed methodology and to validate our computer code.

The paper is organized as follows. We present the governing equations in Section 2. In Section 3 the weak formulation of the problem is stated. A second order time discretization scheme is proposed in Section 4 together with the definition of the characteristics curves associated with the velocity field and the introduction of a second order approximation of them. Section 5 discusses the fully discretized scheme using finite elements spaces. In Section 6, the two dimensional motion of a fluid in a square cavity whose vertical walls are maintained at different temperatures is solved and the numerical results compared with those given in [14].

2. Mathematical model

The governing equations of fluid flow are conservation of mass, momentum and energy. Let us assume our fluid is viscous, incompresible, Newtonian and Boussinesq-approximated. Thus, the equations are given as (see for instance [9], [19], [28])

Continuity:

$$\frac{\partial u^*}{\partial x_1^*} + \frac{\partial v^*}{\partial x_2^*} = 0. \tag{1}$$

Momentum:

$$\frac{\partial \mathbf{v}^*}{\partial t^*} + \text{grad}^*\mathbf{v}^*\mathbf{v}^* + \text{grad}^*\pi_E^* = -\frac{\alpha(\triangle\theta)_0 L^3}{\lambda^2}\theta^*\mathbf{g} + \frac{\eta}{\rho\lambda}\triangle^*\mathbf{v}^*. \tag{2}$$

Energy:

$$\frac{\partial \theta^*}{\partial t^*} + \mathbf{v}^* \cdot \text{grad}^*\theta^* = \triangle^*\theta^*. \tag{3}$$

In the above equations, the following nondimensionalization was employed:

$$\begin{gathered} x_1^* = \frac{x_1}{L} \qquad x_2^* = \frac{x_2}{L} \qquad u^* = \frac{uL}{\lambda} \qquad v^* = \frac{vL}{\lambda} \qquad t^* = \frac{t\lambda}{L^2} \\ \pi_E^* = \frac{\pi_E L^2}{\rho\lambda^2} \qquad \theta^* = \frac{\theta - \theta_0}{\theta_w - \theta_0} = \frac{\theta - \theta_0}{(\triangle\theta)_0} \qquad \rho^* = \frac{\rho}{\rho} = 1, \end{gathered} \tag{4}$$

where L is a suitable characteristic length, $\lambda = \frac{k}{\rho c_\pi}$ is the thermal diffusivity and θ_w is a characteristic temperature on the boundary.

Notations are quite standard,

ρ: density,

$\mathbf{v}^*$: nondimensional velocity vector (u^*, v^*),

π_E^*: nondimensional fluctuation of pressure,

c_π: specific heat at constant pressure,

η: dynamic viscosiy,

θ^*: nondimensional temperature

k: thermal conductivity,

α: coefficient of volumetric thermal expansion at constant pressure, namely,

$$\alpha = -\frac{1}{\rho}\left(\frac{\partial \rho}{\partial \theta}\right)_\pi.$$

Then, the dimensionless parameters involved in the model are

$$\frac{g\alpha(\triangle\theta)_0 L^3}{\lambda^2} \text{ and } Pr := \frac{\eta}{\rho\lambda} = \frac{\nu}{\lambda}, \tag{5}$$

where $\nu = \frac{\eta}{\rho}$ is the kinematic viscosity.

The second parameter, Pr, is the *Prandtl number* approximating the ratio between momentum diffusivity (i.e. viscosity) and thermal diffusivity.

The first parameter can be written as

$$\frac{g\alpha(\triangle\theta)_0 L^3}{\lambda^2} = \frac{g\alpha(\triangle\theta)_0 L^3}{3\lambda\nu}\frac{\nu}{\lambda} = RaPr, \tag{6}$$

where

$$Ra := \frac{g\alpha(\triangle\theta)_0 L^3}{\lambda\nu}, \tag{7}$$

is the *Rayleigh number*, which is a dimensionless number associated with the heat transfer within the fluid. It measures the ratio between the buoyancy force and the viscous force. When the Rayleigh number is below a critical value, heat transfer is primarily in the form of conduction; when it exceeds this critical value, heat transfer is primarily in the form of convection. Moreover, in the last case, if Rayleigh number exceeds certain threshold the flow is unstable. This instability, called Rayleigh-Bénard instability, appears when there is a coupling between the dynamic field and the thermal field (see for instance [28]).

3. Weak Formulation

In what follows we drop the $*$ superscript for the sake of simplicity.
We consider an initial-boundary value problem in a domain $\Omega \subset \mathbb{R}^2$ with boundary Γ. Let us suppose that the velocity and the temperature are given at initial time, namely,

$$\mathbf{v}(\mathbf{x}, 0) = \mathbf{v}_0(\mathbf{x}), \tag{8}$$

$$\theta(\mathbf{x}, 0) = \theta_0(\mathbf{x}). \tag{9}$$

Besides we impose the boundary condition

$$\mathbf{v} = \mathbf{0} \quad \text{on } \Gamma,$$

to the motion equation. For the energy equation we consider mixed boundary conditions: let us decompose the boundary Γ into two disjoint parts, Γ_D and Γ_N, and suppose the temperature is given on Γ_D while the heat flux is prescribed on Γ_N. That is,

$$\theta = \theta_D \quad \text{on } \Gamma_D \times (0, t_f)\,, \tag{10}$$

$$\frac{\partial\theta}{\partial\mathbf{n}} = g_N \quad \text{on } \Gamma_N \times (0, t_f)\,, \tag{11}$$

where $\mathbf{n}$ is the outward unit normal vector to Γ_N, and θ_D and g_N are given scalar functions. Let us recall the definition of the Hilbert spaces $H^1(\Omega)$ and $L^2(\Omega)$:

$$L^2(\Omega) = \left\{ f : \Omega \to \mathbb{R} \text{ measurable}, \int_\Omega f^2 d\mathbf{x} < \infty \right\}, \tag{12}$$

$$H^1(\Omega) = \left\{ f : \Omega \to \mathbb{R} \text{ measurable}, \ f, \ \frac{\partial f}{\partial x_i} \in L^2(\Omega), \ i = 1, 2 \right\}, \tag{13}$$

and denote by $H^1_{\Gamma_D}(\Omega)$ the closed subspaces of $H^1(\Omega)$ defined by

$$H^1_{\Gamma_D}(\Omega) = \left\{ z \in H^1(\Omega) \,/ z|_{\Gamma_D} = 0 \right\}.$$

We also introduce the notations

$$\mathbf{H}^1(\Omega) = (H^1(\Omega))^2,$$
$$\mathbf{H}^1_\Gamma(\Omega) = \{\mathbf{w} \in \mathbf{H}^1(\Omega) : \ \mathbf{w} = 0 \text{ on } \Gamma\}.$$

Now, multiplying equation (2) by a test function $\mathbf{w} \in \mathbf{H}^1_\Gamma(\Omega)$, integrating in Ω and applying a Green's formula we easily get a weak formulation for the motion equation. Similarly, multiplying (1) by a test function $q \in L^2(\Omega)$ and integrating in Ω we obtain a weak formulation for the incompressibility equation. The whole problem is the following:

PM.– *Find* $\mathbf{v}(\cdot,t) \in \mathbf{H}^1_\Gamma(\Omega)$ *and* $\pi_E(\cdot,t) \in L^2(\Omega)$ *such that*

$$\int_\Omega (\mathbf{v}' + \operatorname{grad}\mathbf{v}\mathbf{v}) \cdot \mathbf{w}\, d\mathbf{x} + Pr \int_\Omega \operatorname{grad}\mathbf{v} \cdot \operatorname{grad}\mathbf{w}\, d\mathbf{x} - \int_\Omega \pi_E \operatorname{div}\mathbf{w}\, d\mathbf{x} \tag{14}$$

$$= \int_\Omega \mathbf{b} \cdot \mathbf{w}\, d\mathbf{x},\ \forall \mathbf{w} \in \mathbf{H}^1_\Gamma(\Omega),\ \forall t \in (0,t_f),$$

$$\int_\Omega \operatorname{div}\mathbf{v} q\, d\mathbf{x} = 0,\ \forall q \in L^2(\Omega),\ \forall t \in (0,t_f), \tag{15}$$

$$\mathbf{v}(\mathbf{x},0) = \mathbf{v}_0(\mathbf{x}) \text{ in } \Omega, \tag{16}$$

where $\mathbf{b} = RaPr\theta \cdot (0,1)$.

Analogously, multiplying the heat equation (3) by a test function $z \in H^1_{\Gamma_D}(\Omega)$, using a Green's formula and taking into account the boundary condition (11) we get the following weak formulation:

PE.– *Find a function* $\theta(\cdot,t) \in H^1(\Omega)$ *such that* $\theta(\cdot,t) = \theta_D(\cdot,t)$ on Γ_D and

$$\int_\Omega (\theta' + \operatorname{grad}\theta \cdot \mathbf{v})\, z\, d\mathbf{x} + \int_\Omega \operatorname{grad}\theta \cdot \operatorname{grad} z\, d\mathbf{x} = \int_{\Gamma_N} g_N z\, d\Gamma, \tag{17}$$

$$\forall z \in H^1_{\Gamma_D}(\Omega), \forall t \in (0,t_f),$$

$$\theta(\mathbf{x},0) = \theta_0(\mathbf{x}). \tag{18}$$

4. Time discretization

In this section we consider a second order characteristics scheme for time semidiscretization of problems **PM** and **PE**.

First, we introduce a second order approximation of the total derivative of $\mathbf{v}$ and θ by using a three points formula. Then, we propose a second order approximation of the characteristics curves.

4.1. Characteristic curves

For a field ϕ, we denote by $\dot{\phi}$ the material time derivative. It is defined by

$$\dot{\phi}(\mathbf{x},t) := \frac{\partial}{\partial t}\phi(\mathbf{X}(\mathbf{p},t),t)|_{\mathbf{p}=\mathbf{P}(\mathbf{x},t)}, \tag{19}$$

where $\mathbf{X}$ is the motion corresponding to the velocity $\mathbf{v}$ and $\mathbf{P}$ its reference map. We recall that, according to the standard formalism of continuum mechanics, $\mathbf{x} = \mathbf{X}(\mathbf{p},t)$ is the position at time t of the material point $\mathbf{p}$, while the reference map $\mathbf{P}(\mathbf{x},t)$ yields the material point located at position $\mathbf{x}$ at time t. If φ is a scalar field then

$$\dot{\varphi} = \frac{\partial \varphi}{\partial t} + \mathbf{v} \cdot \operatorname{grad}\varphi, \tag{20}$$

while for a vector field $\boldsymbol{\varphi}$ we have

$$\dot{\boldsymbol{\varphi}} = \frac{\partial \boldsymbol{\varphi}}{\partial t} + \operatorname{grad} \boldsymbol{\varphi}\, \mathbf{v}. \tag{21}$$

Let us introduce the characteristic curves, which are simply the trajectories of the motion associated with the velocity field $\mathbf{v}$. Thus, for given $(\mathbf{x}, t) \in \overline{\Omega} \times [0, t_f]$ the characteristic curve through $(\mathbf{x}, t)$ is defined as the vector function

$$\begin{array}{rccc} \chi(\mathbf{x}, t; \cdot): & (0, t_f) & \longrightarrow & \mathbb{R}^2 \\ & \tau & \longrightarrow & \chi(\mathbf{x}, t; \tau), \end{array} \tag{22}$$

which can be obtained by solving the initial value problem

$$\left\{ \begin{array}{rcl} \dfrac{\partial \chi}{\partial \tau}(\mathbf{x}, t; \tau) & = & \mathbf{v}\left(\chi(\mathbf{x}, t; \tau), \tau\right), \\ \chi(\mathbf{x}, t; t) & = & \mathbf{x}. \end{array} \right. \tag{23}$$

It represents the trajectory described by a material point that is placed at position $\mathbf{x}$ at time t and is driven by the velocity field $\mathbf{v}$. More precisely, $\chi(\mathbf{x}, t; \tau) = \mathbf{X}(\mathbf{P}(\mathbf{x}, t), \tau)$. By using function χ, we can write an alternative expression for the material time derivative of a field ϕ at $(\mathbf{x}, t)$. Indeed, we have

$$\dot{\phi}(\mathbf{x}, t) := \frac{\partial}{\partial t} \phi(\mathbf{X}(\mathbf{p}, t), t)|_{\mathbf{p}=\mathbf{P}(\mathbf{x},t)} = \frac{\partial}{\partial \tau} [\phi(\chi(\mathbf{x}, t; \tau), \tau)]_{|_{\tau=t}}. \tag{24}$$

For the time variable, we introduce the number of time steps, N, and the time step $\Delta t = t_f/N$, obtaining the uniform mesh of $(0, t_f)$:

$$t^n = n\Delta t, \quad 0 \leq n \leq N. \tag{25}$$

The solution will be approximated at times t^n, $n = 1, 2, \ldots, N$. Throughout this work, we use the standard notation $\psi^n(\mathbf{x})$ to denote an approximation of $\psi(\mathbf{x}, t_n)$.

In order to discretize the material time derivative in equations (14) and (17) we propose the following second-order backward approximation

$$y'(t^{n+1}) = \frac{3y(t^{n+1}) - 4y(t^n) + y(t^{n-1})}{2\Delta t} + O\left(\Delta t^2\right), \tag{26}$$

for $n \geq 1$ and, for $n = 0$, the first order backward Euler formula, namely,

$$y'(t^1) = \frac{y(t^1) - y(t^0)}{\Delta t} + O\left(\Delta t\right). \tag{27}$$

Moreover, for $x \in \Omega$ let $\chi^n(\mathbf{x})$ and $\tilde{\chi}^{n-1}(\mathbf{x})$ be defined by

$$\chi^n(\mathbf{x}) := \chi(\mathbf{x}, t^{n+1}; t^n), \quad n = 0, \ldots, N-1, \tag{28}$$

$$\tilde{\chi}^{n-1}(\mathbf{x}) := \chi(\mathbf{x}, t^{n+1}; t^{n-1}), \quad n = 1, \ldots, N-1. \tag{29}$$

We notice that

$$\tilde{\chi}^{n-1}(\mathbf{x}) = \chi^{n-1}(\chi^n(\mathbf{x})). \tag{30}$$

Let us introduce the following time semidiscretizations of problems **PM** and **PE**.

For $n = 0$:

PMD^1.– Find a vector field $\mathbf{v}^1 \in \mathbf{H}^1_\Gamma(\Omega)$ and a scalar field $\pi^1_E \in L^2(\Omega)$ such that

$$\begin{aligned} &\frac{1}{\Delta t}\int_\Omega \mathbf{v}^1\cdot\mathbf{w}\,d\mathbf{x} + Pr\int_\Omega \operatorname{grad}\mathbf{v}^1\cdot\operatorname{grad}\mathbf{w}\,d\mathbf{x} \\ &-\int_\Omega \pi^1_E \operatorname{div}\mathbf{w}\,d\mathbf{x} = \int_\Omega \mathbf{b}^1\cdot\mathbf{w}\,d\mathbf{x} + \frac{1}{\Delta t}\int_\Omega \left(\mathbf{v}^0\circ\chi^0\right)\cdot\mathbf{w}\,d\mathbf{x},\ \forall\mathbf{w}\in\mathbf{H}^1_\Gamma(\Omega), \end{aligned} \tag{31}$$

$$\int_\Omega \operatorname{div}\mathbf{v}^1 q\,d\mathbf{x} = 0,\ \forall q\in L^2(\Omega). \tag{32}$$

For $n \geq 1$:

PMD^{n+1}.– Find two functions $\mathbf{v}^{n+1} \in \mathbf{H}^1_\Gamma(\Omega)$ and $\pi^{n+1}_E \in L^2(\Omega)$ such that

$$\frac{3}{2\Delta t}\int_\Omega \mathbf{v}^{n+1}\cdot\mathbf{w}\,d\mathbf{x} + Pr\int_\Omega \operatorname{grad}\mathbf{v}^{n+1}\cdot\operatorname{grad}\mathbf{w}\,d\mathbf{x} \tag{33}$$

$$\begin{aligned} -\int_\Omega \pi^{n+1}_E \operatorname{div}\mathbf{w}\,d\mathbf{x} &= \int_\Omega \mathbf{b}^{n+1}\cdot\mathbf{w}\,d\mathbf{x} + \frac{2}{\Delta t}\int_\Omega (\mathbf{v}^n\circ\chi^n)\cdot\mathbf{w}\,d\mathbf{x} \\ &-\frac{1}{2\Delta t}\int_\Omega \left(\mathbf{v}^{n-1}\circ\tilde{\chi}^{n-1}\right)\cdot\mathbf{w}\,d\mathbf{x},\ \forall\mathbf{w}\in\mathbf{H}^1_\Gamma(\Omega), \end{aligned}$$

$$\int_\Omega \operatorname{div}\mathbf{v}^{n+1} q\,d\mathbf{x} = 0,\ \forall q\in L^2(\Omega). \tag{34}$$

For $n = 0$:

PED^1.– Find a function $\theta^1 \in H^1(\Omega)$ such that $\theta^1(\mathbf{x}) = \theta_D(\mathbf{x}, t^1)$ on Γ_D and

$$\begin{aligned} \frac{1}{\Delta t}\int_\Omega \theta^1\, z\,d\mathbf{x} + \int_\Omega \operatorname{grad}\theta^1\cdot\operatorname{grad} z\,d\mathbf{x} &= \int_{\Gamma_N} g^1_N z\,d\Gamma \\ &+\frac{1}{\Delta t}\int_\Omega (\theta^0\circ\chi^0) z\,d\mathbf{x},\ \forall z\in H^1_{\Gamma_D}(\Omega). \end{aligned} \tag{35}$$

For $n \geq 1$:

PED^{n+1}.– Find a function $\theta^{n+1} \in H^1(\Omega)$ such that $\theta^{n+1}(\mathbf{x}) = \theta_D(\mathbf{x}, t^{n+1})$ on Γ_D and

$$\begin{aligned} \frac{3}{2\Delta t}\int_\Omega \theta^{n+1}\, z\,d\mathbf{x} + \int_\Omega \operatorname{grad}\theta^{n+1}\cdot\operatorname{grad} z\,d\mathbf{x} &= \int_{\Gamma_N} g^{n+1}_N z\,d\Gamma \\ +\frac{2}{\Delta t}\int_\Omega (\theta^n\circ\chi^n) z\,d\mathbf{x} - \frac{1}{2\Delta t}\int_\Omega (\theta^{n-1}\circ\tilde{\chi}^{n-1}) z\,d\mathbf{x},\ \forall z\in H^1_{\Gamma_D}(\Omega). \end{aligned} \tag{36}$$

In most cases, Cauchy problem (23) cannot be exactly solved. Instead we propose the following numerical approximations of $\chi^n(\mathbf{x})$ and $\tilde{\chi}^{n-1}(\mathbf{x})$ (see [12]):

- For **PMD**[1]: First order explicit Euler scheme

$$\chi_a^0(\mathbf{x}) = \mathbf{x} - \triangle t \mathbf{v}^0(\mathbf{x}). \tag{37}$$

- For **PED**[1]: Second order explicit two-step sheme

$$\chi_a^0(\mathbf{x}) = \mathbf{x} - \triangle t \left(2\mathbf{v}^1(\mathbf{x}) - \mathbf{v}^0(\mathbf{x})\right). \tag{38}$$

- For $n \geq 1$: Second order explicit two-step sheme

$$\chi_a^n(\mathbf{x}) = \mathbf{x} - \left(2\mathbf{v}^n(\mathbf{x}) - \mathbf{v}^{n-1}(\mathbf{x})\right)\left(t^{n+1} - t^n\right), \tag{39}$$

$$\tilde{\chi}_a^{n-1}(\mathbf{x}) = \mathbf{x} - \left(2\mathbf{v}^n(\mathbf{x}) - \mathbf{v}^{n-1}(\mathbf{x})\right)\left(t^{n+1} - t^{n-1}\right). \tag{40}$$

5. Space discretization: finite element method

In this section we propose a space discretization of the above problems **PMD** and **PED** by using finite elements (piecewise quadratic for the thermal problem and piecewise linear + bubble for the fluid dynamics problem).

Let us suppose Ω is a bounded domain in $\mathbb{R}^2$ with a Lipschitz polygonal boundary. Let us consider two suitable families of regular triangulations of $\overline{\Omega}$ to be denoted by τ_h^M for the fluid dynamics problem **PMD** and τ_h^E for the thermal problem **PED**, both consisting of elements K of diameter $\leq h$. Moreover, we assume the latter is compatible with the partition of the boundary into Γ_D and Γ_N.

We define the following polynomial spaces:

$$\begin{aligned}
P_2(K) &= \left\{q_{|_K} : q : \mathbb{R}^2 \longrightarrow \mathbb{R} \text{ polynomial of degree } \leq 2\right\}, \\
P_1(K) &= \left\{q_{|_K} : q : \mathbb{R}^2 \longrightarrow \mathbb{R} \text{ polynomial of degree } \leq 1\right\}, \\
P_b(K) &= \left\{q + \alpha\lambda_4^K : q \in P_1(K)\ ,\ \alpha \in \mathbb{R}\right\},
\end{aligned}$$

being $\lambda_4^K = 27\prod_{i=1}^3 \lambda_i^K$ the bubble function of element K, where $\{\lambda_1^K, \lambda_2^K, \lambda_3^K\}$ denote the barycentric coordinates with respect to the vertices of element K.
We consider the following spaces of finite elements:

$$X_h = \left\{\mathbf{w}_h \in C^0(\Omega)^2 :\ \mathbf{w}_{h|_K} \in P_b(K)^2,\quad \forall K \in \tau_h^M\right\}, \tag{41}$$

$$X_{0h} = \left\{\mathbf{w}_h \in X_h :\ \mathbf{w}_h = \mathbf{0} \text{ on } \Gamma\right\}, \tag{42}$$

$$V_h^1 = \left\{\varphi_h \in C^0(\Omega) :\ \varphi_{h|_K} \in P_1(K),\quad \forall K \in \tau_h^M\right\}, \tag{43}$$

$$V_h^2 = \left\{\varphi_h \in C^0(\Omega) :\ \varphi_{h|_K} \in P_2(K),\quad \forall K \in \tau_h^E\right\}, \tag{44}$$

$$V_{0h}^2 = \left\{\varphi_h \in V_h^2 :\ \varphi_h = 0 \text{ on } \Gamma_D\right\}. \tag{45}$$

In order to obtain fully discrete schemes of problems **PMD** (respectively, **PED**) we use the approximations of functional spaces $\mathbf{H}_\Gamma^1(\Omega)$ and $L^2(\Omega)$ (respectively, $H^1(\Omega)$ and

$H^1_{\Gamma_D}(\Omega)$) given by (42) and (43) (respectively, (44) and (45)).
Thus, we obtain the following fully discrete problems:

PMD^1_h.– Find two functions $\mathbf{v}^1_h \in X_{0h}$ and $\pi^1_{E,h} \in V^1_h$ such that

$$\frac{1}{\Delta t}\int_\Omega \mathbf{v}^1_h \cdot \mathbf{w}_h \, d\mathbf{x} + Pr \int_\Omega \operatorname{grad} \mathbf{v}^1_h \cdot \operatorname{grad} \mathbf{w}_h \, d\mathbf{x} - \int_\Omega \pi^1_{E,h} \operatorname{div} \mathbf{w}_h \, d\mathbf{x} \tag{46}$$
$$= RaPr \int_\Omega (0, \theta^0_h) \cdot \mathbf{w}_h \, d\mathbf{x} + \frac{1}{\Delta t}\int_\Omega \left(\mathbf{v}^0_h \circ \chi^0_{a,h}\right) \cdot \mathbf{w}_h \, d\mathbf{x}, \ \forall \mathbf{w}_h \in X_{0h},$$
$$\int_\Omega \operatorname{div} \mathbf{v}^1_h q_h \, d\mathbf{x} = 0, \ \forall q_h \in V^1_h, \tag{47}$$

with

$$\mathbf{v}^0_h(\mathbf{a}) = \mathbf{v}_0(\mathbf{a}) \ \text{ for all node } \mathbf{a} \text{ of the mesh } \tau^M_h, \tag{48}$$

and where $\chi^0_{a,h}(\mathbf{x}) = \mathbf{x} - \triangle t \mathbf{v}^0_h(\mathbf{x})$.

PMD$^{n+1}_h$.– Find two functions $\mathbf{v}^{n+1}_h \in X_{0h}$ and $\pi^{n+1}_{E,h} \in V^1_h$ such that

$$\frac{3}{2\Delta t}\int_\Omega \mathbf{v}^{n+1}_h \cdot \mathbf{w}_h \, d\mathbf{x} + Pr \int_\Omega \operatorname{grad} \mathbf{v}^{n+1}_h \cdot \operatorname{grad} \mathbf{w}_h \, d\mathbf{x} - \int_\Omega \pi^{n+1}_{E,h} \operatorname{div} \mathbf{w}_h \, d\mathbf{x} \tag{49}$$
$$= RaPr \int_\Omega (0, \theta^{n+1}_h) \cdot \mathbf{w}_h \, d\mathbf{x} + \frac{2}{\Delta t}\int_\Omega \left(\mathbf{v}^n_h \circ \chi^n_{a,h}\right) \cdot \mathbf{w}_h \, d\mathbf{x}$$
$$-\frac{1}{2\Delta t}\int_\Omega \left(\mathbf{v}^{n-1}_h \circ \tilde{\chi}^{n-1}_{a,h}\right) \cdot \mathbf{w}_h \, d\mathbf{x}, \ \forall \mathbf{w}_h \in X_{0h},$$
$$\int_\Omega \operatorname{div} \mathbf{v}^{n+1}_h q \, d\mathbf{x} = 0, \ \forall q_h \in V^1_h, \tag{50}$$

where

$$\chi^n_{a,h}(\mathbf{x}) = \mathbf{x} - \left(2\mathbf{v}^n_h(\mathbf{x}) - \mathbf{v}^{n-1}_h(\mathbf{x})\right)\left(t^{n+1} - t^n\right),$$
$$\tilde{\chi}^{n-1}_{a,h}(\mathbf{x}) = \mathbf{x} - \left(2\mathbf{v}^n_h(\mathbf{x}) - \mathbf{v}^{n-1}_h(\mathbf{x})\right)\left(t^{n+1} - t^{n-1}\right).$$

PED^1_h.– Find a function $\theta^1_h \in V^2_h$ such that

$$\frac{1}{\Delta t}\int_\Omega \theta^1_h \, z_h \, d\mathbf{x} + \int_\Omega \operatorname{grad} \theta^1_h \cdot \operatorname{grad} z_h \, d\mathbf{x} = \int_{\Gamma_N} g^1_N z_h \, d\Gamma \tag{51}$$
$$+\frac{1}{\Delta t}\int_\Omega (\theta^0_h \circ \chi^0_{a,h}) z_h \, d\mathbf{x}, \ \forall z_h \in V^2_{0h},$$

with

$$\theta^0_h(\mathbf{a}) = \theta_0(\mathbf{a}), \ \text{for all node } \mathbf{a} \text{ of the mesh } \tau^E_h, \tag{52}$$

$$\theta^1_h(\mathbf{a}) = \theta_D(\mathbf{a}, t^1) \text{ for all node } \mathbf{a} \text{ on } \Gamma_D, \tag{53}$$

and where $\chi^0_{a,h}(\mathbf{x}) = \mathbf{x} - \triangle t\,(2\mathbf{v}^1_h(\mathbf{x}) - \mathbf{v}^0_h(\mathbf{x}))$.

PED$^{n+1}_h$.– Find a function $\theta^{n+1}_h \in V^2_h$ such that

$$\frac{3}{2\Delta t}\int_\Omega \theta^{n+1}_h\, z_h\, d\mathbf{x} + \int_\Omega \operatorname{grad}\theta^{n+1}_h \cdot \operatorname{grad} z_h\, d\mathbf{x} = \int_{\Gamma_N} g^{n+1}_N z_h\, d\Gamma$$
$$+\frac{2}{\Delta t}\int_\Omega (\theta^n_h \circ \chi^n_{a,h}) z_h\, d\mathbf{x} - \frac{1}{2\Delta t}\int_\Omega (\theta^{n-1}_h \circ \tilde{\chi}^{n-1}_{a,h}) z_h\, d\mathbf{x},\ \forall z_h \in V^2_{0h},$$

with

$$\theta^{n+1}_h(\mathbf{a}) = \theta_D(\mathbf{a}, t^{n+1}) \text{ for all node } \mathbf{a} \text{ on } \Gamma_D, \tag{54}$$

and where

$$\chi^n_{a,h}(\mathbf{x}) = \mathbf{x} - \left(2\mathbf{v}^n_h(\mathbf{x}) - \mathbf{v}^{n-1}_h(\mathbf{x})\right)\left(t^{n+1} - t^n\right),$$
$$\tilde{\chi}^{n-1}_{a,h}(\mathbf{x}) = \mathbf{x} - \left(2\mathbf{v}^n_h(\mathbf{x}) - \mathbf{v}^{n-1}_h(\mathbf{x})\right)\left(t^{n+1} - t^{n-1}\right).$$

Notice that these problems are decoupled.

Remark 5.1. *For a practical implementation of the method we need to use appropriated quadrature formulas to approximate the terms involving the operators $\chi^n_{a,h}$ and $\tilde{\chi}^n_{a,h}$. Some papers in the literature study the influence of quadrature formulas in both stability and consistency errors (see for instance [22], [30] and [11]). In order to reduce the time of calculation we will use quadrature formulas that require a small number of nodes while maintaining the overall order of convergence.*
Hence, in practice, mappings $\chi^n_{a,h}$ and $\tilde{\chi}^n_{a,h}$ will be calculated only for quadrature nodes. This will be specified in Section 6 below. Moreover, from the definition of $\chi^n_{a,h}$ (respectively, $\tilde{\chi}^n_{a,h}$), we deduce that for some quadrature nodes, $a_i,\ i = 1, \ldots, num$, (respectively, $\tilde{a}_i,\ i = 1, \ldots, \widetilde{num}$), the characteristic curves go out of the computational domain. In this case, we consider the first order Taylor expansion of $\mathbf{v}^n_h$ and θ^n_h around a_i (respectively, $\tilde{a}_i$) to approximate $(\mathbf{v}^n_h \circ \chi^n_{a,h})(a_i)$ and $(\theta^n_h \circ \chi^n_{a,h})(a_i)$ (respectively, $(\mathbf{v}^n_h \circ \tilde{\chi}^n_{a,h})(\tilde{a}_i)$ and $(\theta_h \circ \tilde{\chi}^n_{a,h})(\tilde{a}_i)$), namely,

$$\theta^n_h(\chi^n_{a,h}(a_i)) \simeq \theta^n_h(a_i) + \operatorname{grad}\theta^n_h(a_i) \cdot (\chi^n_{a,h}(a_i) - a_i),$$
$$\theta^n_h(\tilde{\chi}^n_{a,h}(\tilde{a}_i)) \simeq \theta^n_h(\tilde{a}_i) + \operatorname{grad}\theta^n_h(\tilde{a}_i) \cdot (\tilde{\chi}^n_{a,h}(\tilde{a}_i) - \tilde{a}_i),$$
$$\mathbf{v}^n_h(\chi^n_{a,h}(a_i)) \simeq \mathbf{v}^n_h(a_i) + \operatorname{grad}\mathbf{v}^n_h(a_i)(\chi^n_{a,h}(a_i) - a_i),$$
$$\mathbf{v}^n_h(\tilde{\chi}^n_{a,h}(\tilde{a}_i)) \simeq \mathbf{v}^n_h(\tilde{a}_i) + \operatorname{grad}\mathbf{v}^n_h(\tilde{a}_i)(\tilde{\chi}^n_{a,h}(\tilde{a}_i) - \tilde{a}_i).$$

6. Numerical tests. Problem description

In order to assess the performance of the above numerical methods we solve two test problems. The first one is the *rotating Gaussian hill*. The second one is a natural convection problem in a square cavity whose vertical walls are maintained at different temperatures.

Example 1: the rotating Gaussian hill

This is a convection-diffusion problem with variable coefficients (see for instance [27] and [11]) aiming to compare the computed solution by using first order characteristics combined with piecewise linear finite elements with the one obtained from the second order method proposed in this paper.
The spatial domain is $\Omega = (-1., 1.) \times (-1., 1.)$ and $t_f = 2\pi$. The "thermal conductivity" is the tensor $k_{ij} = \sigma_1 \delta_{ij}$ with σ_1 given below. Moreover, $\mathbf{v} = (-x_2, x_1)$ and the source term $f = 0$. We also impose appropriate Dirichlet boundary conditions and initial condition such that the solution of the problem is

$$\theta(x_1, x_2, t) = \frac{\sigma_2}{\sigma_2 + 4\sigma_1 t} \exp\left\{ -\frac{(\overline{x}(t) - x_c)^2 + (\overline{y}(t) - y_c)^2}{\sigma_2 + 4\sigma_1 t} \right\} \tag{55}$$

where

$$\begin{aligned} \overline{x} = x_1 \cos t + x_2 \sin t,\ \overline{y} = -x_1 \sin t + x_2 \cos t, \\ (x_c, y_c) = (0.25, 0),\ \sigma_1 = 0.001,\ \sigma_2 = 0.01. \end{aligned} \tag{56}$$

Moreover, the velocity field does not vanish on the boundary, thus we have artificially imposed $\theta = 0$ wherever the characteristic curves go out of the computational domain.

Example 2: a steady state natural convection problem

We consider a two-dimensional problem of natural convection in a square cavity of side L. For numerical simulation we use the Boussinesq approximate model (see Section 2), with Prandtl number $Pr = 0.71$. The left and right walls are maintained at temperatures θ_L and θ_R, respectively, where $\theta_L > \theta_R$, and the horizontal walls are adiabatic (i. e. insulated, there is no heat transfer through these walls). The problem is depicted in Figure 1, where we use the notation introduced in Section 2. The solution to this problem, namely, velocity, temperature and pressure were obtained for Rayleigh number in the range $10^3 \leq Ra \leq 10^7$.

By using the nondimensionalizations given in (4), the motion and the heat transfer are governed by the nondimensional equations (1)-(3).
These equations are subjected to the following initial conditions (see Figure 1),

$$\theta = u = v = 1, \qquad \text{at } t = 0, \tag{57}$$

and to the boundary conditions for $t > 0$,

$$u = v = 0 \quad \theta = 1, \text{ for} \quad x_1 = 0, \quad 0 \leq x_2 \leq 1, \tag{58}$$

$$u = v = 0 \quad \theta = 0, \text{ for} \quad x_1 = 1, \quad 0 \leq x_2 \leq 1, \tag{59}$$

$$u = v = \frac{\partial \theta}{\partial x_2} = 0, \text{ for} \quad x_2 = 0, 1, \quad 0 < x_1 < 1. \tag{60}$$

This problem has been solved by the methods presented in the previous sections. We have integrated in time step by step as far as to obtain a steady solution. More specifically,

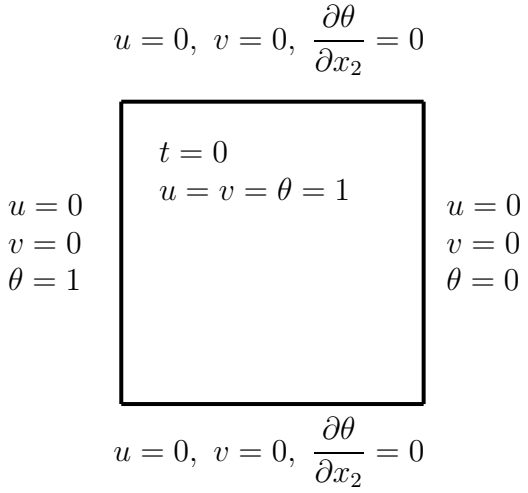

Figure 1: Initial and boundary conditions.

the following test has been satisfied in all simulations:

$$\frac{|\ \mathbf{v}_h^{n+1} - \mathbf{v}_h^n|_\infty}{\Delta t} \leq 10^{-8},$$

where $|\cdot|_\infty$ denotes the maximum norm.

7. Numerical results

In practice the inner products in the Galerkin formulation are calculated using numerical quadrature. In general this adds some terms to the final error estimates and, in some cases, it produces the loss of unconditional stability. There are several papers in the literature analyzing the effect of numerical integration in Lagrange-Galerkin methods (see [22], [30], [26], [18], [32], [11]). In particular, in [22] Fourier analysis is developed for the classical Lagrange-Galerkin method for piecewise linear finite element, applied to the one dimensional linear convection equation and combined with several quadrature formulas. Unconditional stability has been shown for trapezoidal rule and unconditional instability has been proved when the mass matrix is exactly integrated and the term of characteristics is approximated by using trapezoidal rule (Lemma 2.4 in [22]). Throughout Appendix A we develop an analogous approach for the classical Lagrange-Galerkin method for piecewise linear finite element with the strategy given in (61) combined with vertex quadrature in the first term on the right side (see [23] for more details), applied to the one dimensional linear convection equation. For this scheme conditional stability is shown.

Thanks to the experience gained in the use of the proposed numerical methods for academical test examples, we have reached the conclusion that the most suitable quadrature formulas are the following:

- The integrals corresponding to the motion equation are exactly calculated except for the *terms of characteristics* which has been approximated by using first the

following decomposition:

$$\int_K (\mathbf{v}_h^m \circ \chi_{a,h}^m) \cdot \mathbf{w}_h \, d\mathbf{x} = \int_K (\mathbf{v}_h^m \circ \chi_{a,h}^m - \mathbf{v}_h^m) \cdot \mathbf{w}_h \, d\mathbf{x} + \int_K \mathbf{v}_h^m \cdot \mathbf{w} \, d\mathbf{x}. \tag{61}$$

Then the first integral on the right-hand side is calculated by using a quadrature formula exact for polynomials of degree 1 and the second one by using exact integration. The same technique is used by replacing χ_a^m with $\tilde{\chi}_a^{n-1}$. With this method we have obtained satisfactory results, as Example 1 shows. A Fourier stability analysis showing conditional stability has been shown in the Appendix. Moreover, we recall that using the vertex quadrature directly in the characteristics term (i.e. in the term on the left-hand side of (61)) leads to an unconditionally unstable scheme (see [22]). Another alternative leading to an unconditionally stable scheme consists of using the vertex quadrature formula not only in the characteristics term but also in the mass term (see again [22]). In Example 1 we show numerical results comparing these methods in the scalar case.

- The integrals corresponding to the energy equation were approximated by using an exact quadrature formula for polynomials of degree 2.

Firstly, we show numerical results for the problem of the rotating Gaussian hill and then for the problem of natural convection described above.

Example 1

For this problem we compare numerical results obtained with the classical characteristics method, denoted by $(\mathcal{SLG})_1$ and the second order method described in the present paper for the thermal problem, denoted by $(\mathcal{SLG})_2$. Moreover, we present numerical results showing that with the second order method $(\mathcal{SLG})_2$ the strategy given in (61) lead to more stable schemes than the classical one. This is illustrated in Table 1 which shows the $L^2(\Omega)$ norm of the computed solution for both schemes, when they are combined with an exact quadrature formula for polynomials of degree 2. In particular, in Table 1 we denote by $(\mathcal{SLG})_2$*/classical* the scheme $(\mathcal{SLG})_2$ combined with an exact quadrature formula for polynomials of degree 2 in all the terms, and by $(\mathcal{SLG})_2$*/strategy (61)*, the scheme $(\mathcal{SLG})_2$ with the strategy given in (61) and combined with an exact quadrature formula for polynomials of degree 2 in the first term on the right side of (61).

We have also tested the above strategies for the classical order one method $(\mathcal{SLG})_1$. For this, we have solved the pure convection problem ($\sigma_1 = 0$) in order to keep the case analyzed in the Appendix. The results obtained are presented in Table 2 which shows the $L^2(\Omega)$ norm of the computed solution for the proposed schemes at time $t_f = 2\pi$. More precisely, in Table 2 we denote by $(\mathcal{SLG})_1$*/vertex* the scheme $(\mathcal{SLG})_1$ combined with the vertex quadrature in all the terms, by $(\mathcal{SLG})_1$*/(61)-vertex*, the scheme $(\mathcal{SLG})_1$ with the strategy given in (61) and combined with vertex quadrature in the first term on the right-hand side of (61) and by $(\mathcal{SLG})_1/exact - vertex$ the scheme $(\mathcal{SLG})_1$ combined with quadrature vertex in the characteristics term (i.e. in the term on the left-hand side of (61)) and exact integration in the mass matrix. As predicted by Theorem A.1 and by Lemma 2.4 in [22], the numerical results show that: (1) the scheme $(\mathcal{SLG})_1$*/(61)-vertex*

is conditionally stable; (2) the scheme $(\mathcal{SLG})_1$*/vertex* is unconditionally stable; (3) the scheme $(\mathcal{SLG})_1$*/exact-vertex* is unconditionally instable.

In Figures 2, 3 and 4 we compare the numerical results obtained with the classical characteristics method $(\mathcal{SLG})_1$ and the second order method described above for the thermal problem, $(\mathcal{SLG})_2$, when both are combined with an exact quadrature formula for polynomials of degree 2 in all the terms.

In Figure 2 (top) we have fixed a small time step and shown the $L^\infty((0,t_f);L^2(\Omega))$ error versus $1/h$. In Figure 2 (bottom) we represent the computed $L^\infty((0,t_f);L^2(\Omega))$ error versus the number of time steps for a uniform spatial mesh of 133×133 vertices. We can observe, for fixed h, an increasing error as the time step decreases below a threshold. This is due to the presence of a term $O(h^\alpha/\Delta t)$, added by the quadrature formula to the error.

In Figure 3 we can see the exact solution compared with the computed solutions by using the first order Lagrange-Galerkin method $(\mathcal{SLG})_1$. In Figure 4 the exact solution is compared with the numerical results obtained by using the second order method $(\mathcal{SLG})_2$ proposed in the present paper. In both cases a uniform spatial mesh of 133×133 vertices has been used and we have chosen the number of time step that minimizes $L^\infty((0,t_f);L^2(\Omega))$ error. Clearly, $(\mathcal{SLG})_2$ achieves better results than the corresponding classical first order method.

scheme / time (t)	$(\mathcal{SLG})_2$/classical	$(\mathcal{SLG})_2$/strategy (61)
0	0.1253	0.1253
$2\pi/3$	0.2014	0.1010
$8\pi/3$	17.1745	0.0898
2π	1972.1986	0.1208

Table 1: $L^2(\Omega)$ norm of the computed solution with $h=1/25$, $\Delta t=\pi/60$, for Example 1 with $\sigma_1=0.001$.

scheme / Δt	$(\mathcal{SLG})_1$/vertex	$(\mathcal{SLG})_1$/exact-vertex	$(\mathcal{SLG})_1$/(61)-vertex
$\pi/100$	0.1035	$2.2056E+108$	$1.0834E+045$
$\pi/150$	0.1032	Infinity	420.5610
$\pi/175$	0.1031	Infinity	0.1029
$\pi/200$	0.1030	Infinity	0.1029
$\pi/1000$	0.1027	Infinity	0.1025

Table 2: $L^2(\Omega)$ norm of the computed solution with $h=1/133$ at time $t_f=2\pi$, for Example 1 with $\sigma_1=0$.

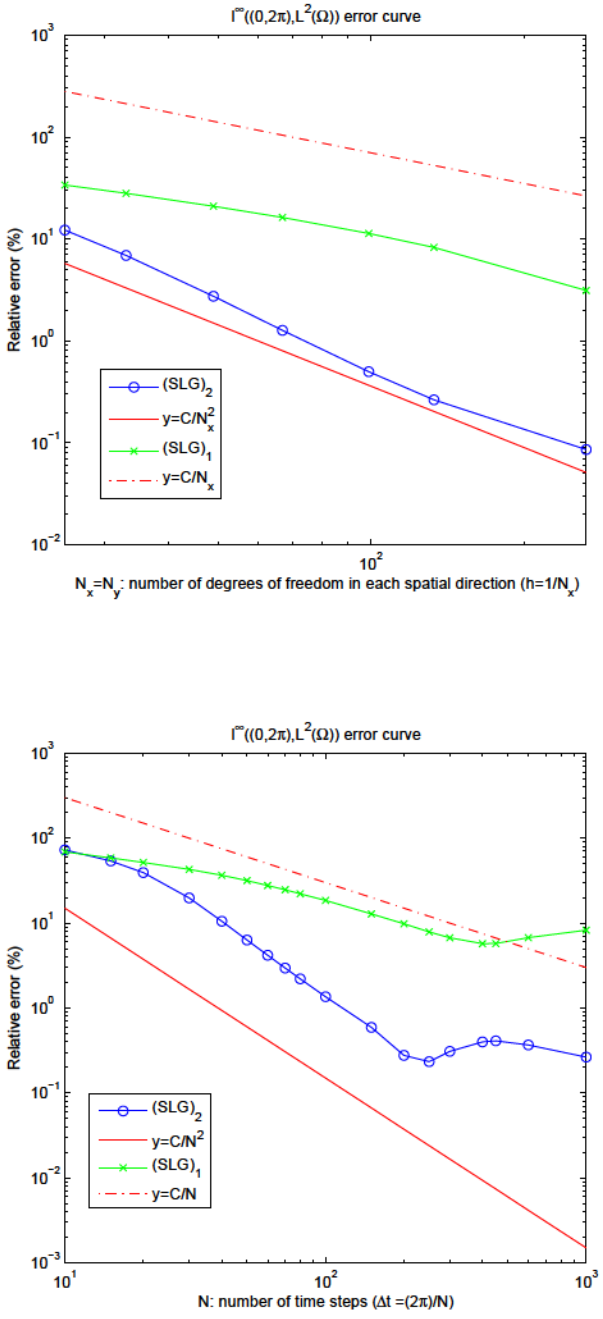

Figure 2: Computed $L^{\infty}\left((0,t_f);L^2(\Omega)\right)$ errors, in log-log scale, for Example 1. On the top errors versus $1/h$. On the bottom errors versus the number of time steps.

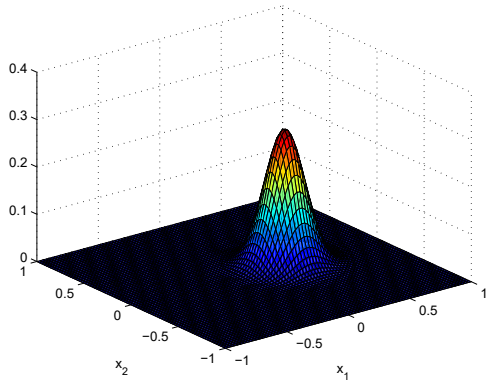

Exact solution.

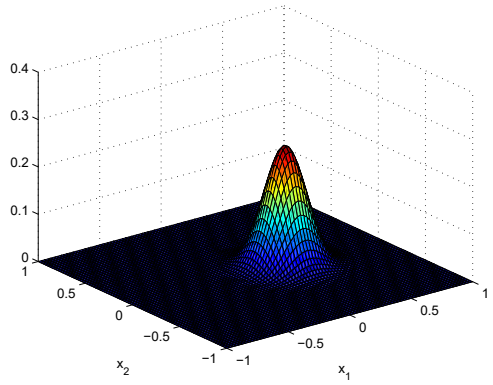

First order $(\mathcal{SLG})_1$ computed solution.

Figure 3: Exact and computed solution of **Example 1** at time $t_f = 2\pi$ with first order $(\mathcal{SLG})_1$ and mesh parameters $N_{x_1} = N_{x_2} = 133$ (in each direction) and $\Delta t = \pi/200$.

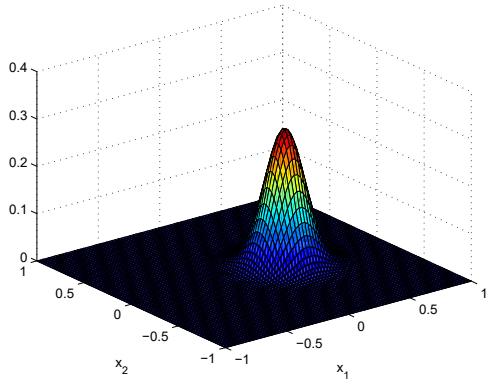

Exact solution.

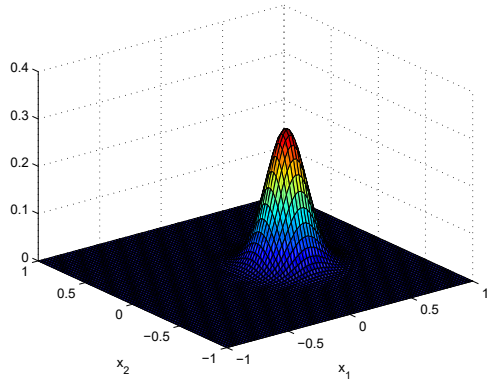

Second order $(\mathcal{SLG})_2$ computed solution.

Figure 4: Exact and computed solution of **Example 1** at time $t_f = 2\pi$ with second order $(\mathcal{SLG})_2$ and mesh parameters $N_{x_1} = N_{x_2} = 133$ (in each direction) and $\Delta t = \pi/125$.

Example 2

We study the problem of natural convection described in Section 6.

For $Ra = 10^3$ and $Ra = 10^4$, the solutions were computed using several uniform meshes of 9×9, 17×17 and 33×33 vertices (for the motion equation), and 13×13, 25×25 and 49×49 vertices (for the energy equation). For higher Ra values, finer meshes were necessary. To be more precise, for $Ra \geq 10^5$ the solution we present here was obtained using non-uniform meshes of 201×201 vertices which are finer near the hot and cold walls. For $Ra = 10^3$, $Ra = 10^4$ the solutions were computed using uniform meshes with $h = 0.02$.

From the point of view of applications one parameter of practical importance is the heat rate convected from the wall to the fluid. This can be obtained by using the dimensionless magnitudes. More precisely, the local heat flux in the horizontal direction at any

point in the cavity is

$$Nu\,(x_1, x_2) = u\theta - \frac{\partial \theta}{\partial x_1}.$$

In the present work we calculate quantities which can be readily compared. In particular, we calculate the average Nusselt number on the vertical boundary of the cavity at $x_1 = 0$:

$$Nu_0 = \int_0^1 Nu(0, x_2)\, dx_2,$$

and the average Nusselt number in the whole cavity:

$$\overline{Nu} = \int_0^1 \int_0^1 Nu(x_1, x_2)\, dx_2\, dx_1.$$

These integrals are computed by using compound Simpson quadrature. We calculate the average Nusselt number on the vertical boundary of the cavity at $x_1 = 0$ for different temporal/spatial meshes to arrive at a grid-independent solution for $Ra = 10^3$. The results are summarized in Table 3. Table 4 shows the error obtained comparing these values with the ones obtained by de Vahl Davis [14] which are taken as reference values. We observe an order of the error varying from 1.43 to 1.80. Moreover, due to numerical quadrature a $O(1/\Delta t)$ term is observed fixed h (see [24]). The calculated averages of the

Meshes / Δt	**12\8**	**24\16**	**48\32**
0.04	1.09080	1.11204	1.11822
0.02	1.08521	1.10910	1.11620
0.01	1.08335	1.10589	1.11473
0.005	1.08276	1.10481	1.11308
0.0025	1.08263	1.10437	1.11258
0.00125	1.08259	1.10426	1.11233
0.000625	1.08259	1.10423	1.11227
0.0003125	1.08258	1.10423	1.11226
0.00015625		1.10423	
0.000078125	1.08259		

Table 3: Grid sensitivity studies : convergence of the average Nusselt number on the vertical boundary of the cavity at $x_1 = 0$, for $Ra = 10^3$.

Nusselt number in the whole cavity are summarized in Table 5 together with the same values from another investigations, for the purpose of comparison.

Meshes / Δt	**12\8**	**24\16**	**48\32**
0.04	$2.62E-02$	$4.96E-03$	$1.23E-03$
0.02	$3.18E-02$	$7.89E-03$	$7.95E-04$
0.01	$3.36E-02$	$1.11E-02$	$2.26E-03$
0.005	$3.42E-02$	$1.22E-02$	$3.91E-03$
0.0025	$3.44E-02$	$1.26E-02$	$4.42E-03$
0.00125	$3.44E-02$	$1.27E-02$	$4.66E-03$
0.000625	$3.44E-02$	$1.28E-02$	$4.72E-03$
0.0003125	$3.44E-02$	$1.28E-02$	$4.74E-03$
0.00015625		$1.28E-02$	$4.74E-03$
0.000078125	$3.44E-02$		

Table 4: Error for the average Nusselt number on the vertical boundary of the cavity at $x_1 = 0$ for $Ra = 10^3$.

Ref / **Ra**	Ref. [14]	Ref. [21]	Ref. [20]	Ref. [33]	Present study
$\mathbf{10^3}$	1.118	1.117	1.074	1.117	1.112
$\mathbf{10^4}$	2.243	2.243	2.084	2.254	2.198
$\mathbf{10^5}$	4.519	4.521	4.3	4.598	4.465
$\mathbf{10^6}$	8.800	8.806	8.743	8.976	8.783
$\mathbf{10^7}$	–	16.40	13.99	16.656	16.46

Table 5: Comparison of the average Nusselt numbers throughout the cavity.

Isotherm, isovelocity, isovorticity and isopressure contours are plotted in Figure 5.

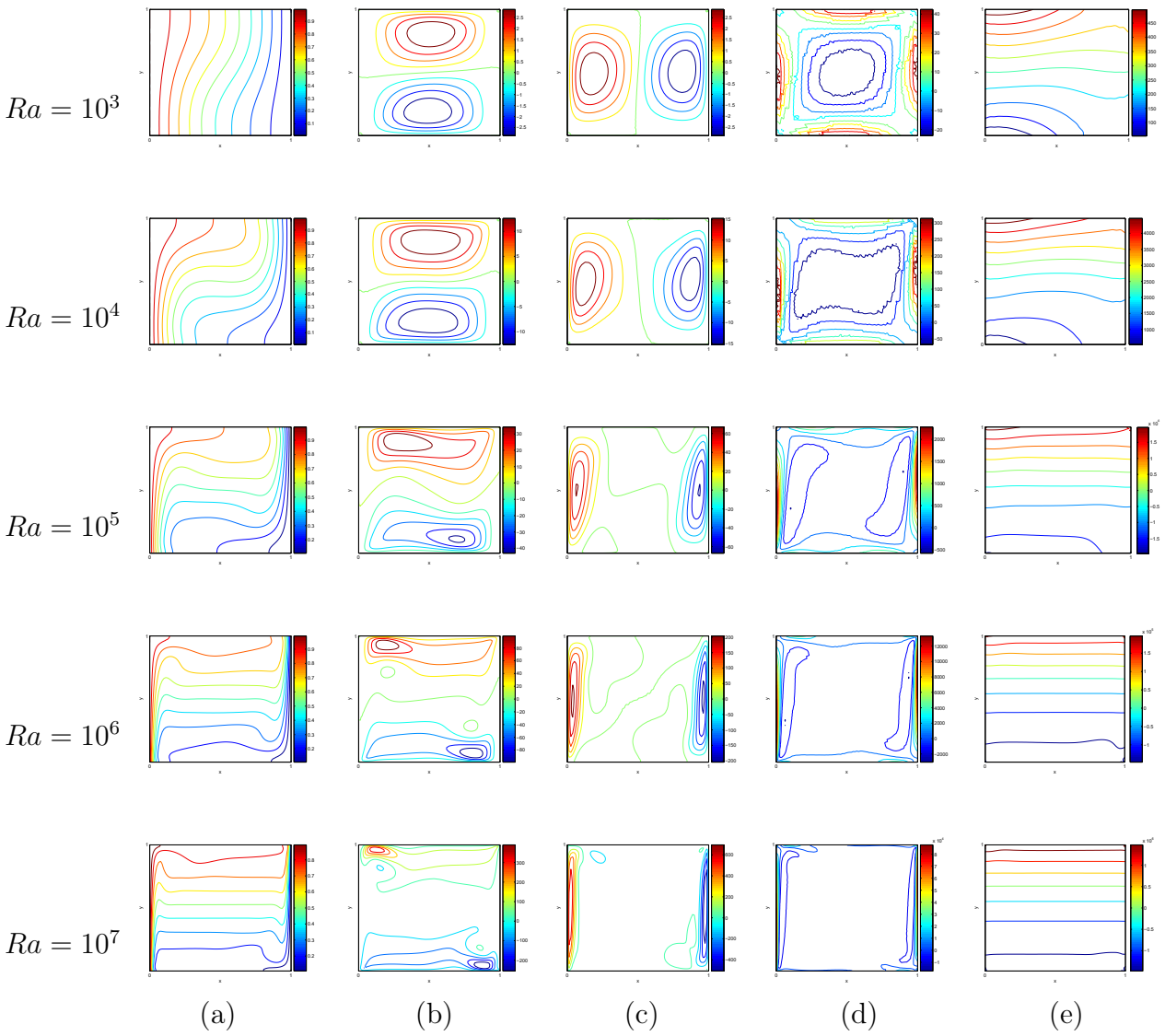

Figure 5: Natural-convection patterns simulated for $10^3 \leq Ra \leq 10^7$:(a) isotherms;(b) iso$-u$ contours;(c) iso$-v$ contours; (d) isovorticity contours; (e) isopressure contours.

The problem of natural convection in a square cavity with differentially heated vertical walls has two different kinds of flow: (1) due to the boundary conditions; (2) a recirculating motion in the core region. The first is the most important for higher Ra values, whereas the second dominates for lower Ra numbers. These features can be observed in Figure 5. Two horizontal eddies can be seen in the iso$-u$ contours, for $Ra = 10^3$ and $Ra = 10^4$. For higher Rayleigh number these eddies are stretched to the top left and bottom right corners. Something similar occurs for the iso$-v$ contours; in this case two vertical eddies appear for $Ra = 10^3$. These vertical eddies become closer to the hot and cold walls with increasing Rayleigh numbers. The different regimes of flow are well depicted in the isotherms of the Figure 5. At the lowest Rayleigh, the temperature is nearly linear with the vertical contours; the heat transfer is almost entirely in the form of conduction.

Increasing Ra, convection becomes increasingly prominent. The horizontal temperature gradient becomes smaller which shows that heat transfer by conduction is reducing. For $Ra = 10^5$ and higher, the growth of the boundary layer along the wall dominates, the hot fluid has been carried to the cold wall, and viceversa. As Ra increases, the contours gradually transform into horizontal except for the immediate neighborhood of the hot and cold walls which remain parallel to the isothermal vertical walls.

8. Conclusions

In the present work a higher order characteristics finite element method for numerical discretization of natural convection problems has been introduced. For validation purposes, a numerical study of the problem of bouyancy-driven flow in a square cavity with differentially heated side walls has been presented. A comparative analysis of the obtained results with the ones appearing in the literature is developed. Convergence of the solution has been shown by comparison with a previous benchmark solution. There is a very good agreement of the isotherm, isovelocity, and isovorticity contours. We have reported numerical solutions for Rayleigh numbers in the range $10^3 \leq Ra \leq 10^7$, while the benchmark solution given in [14] was presented for $10^3 \leq Ra \leq 10^6$.

A. Appendix

In this section, we analyze the stability of the classical Lagrange-Galerkin method combined with the technique given in (61), applied to the one-dimensional linear convection equation with constant coefficients, namely,

$$\theta_t + v\frac{d\theta}{dx} = 0, \tag{62}$$

with v constant.
Thus, we consider the following scheme

$$\int_\Omega \theta_h^{n+1}\psi_j\,dx = \int_\Omega (\theta_h^n \circ \chi_a - \theta_h^n)\psi_j\,dx + \int_\Omega \theta_h^n\psi_j\,dx, \tag{63}$$

where $\chi_a(x) = x - v\Delta t$ and ψ_j is the $j-th$ basis function of the space finite element. In the following, we develop Fourier analysis to study the stability of scheme (63). We recall the definition of the Courant number: $\mu = |v|\Delta t/h$.

Theorem A.1. *The scheme (63) with linear elements on a uniform mesh is stable for CLF numbers $\mu \leq 1/3$ when the mass matrix and the second term on the right side are both exactly integrated and the first term on the right side is evaluated by vertex quadrature.*

Proof. Firstly, let us compute the terms appearing in the $j-th$ equation. We use the notation $\theta_j^n := \theta_h(x_j, t_n)$ for a meshpoint (x_j, t_n).
The mass matrix and the second term on the right side of (63) are both exactly integrated

giving rise to

$$\begin{aligned}\int_\Omega \theta_h^{n+1}\psi_j\,dx &= \frac{h}{6}\left(\theta_{j+1}^{n+1}+4\theta_j^{n+1}+\theta_{j-1}^{n+1}\right)=\frac{h}{6}\left(\theta_{j+1}^{n+1}-2\theta_j^{n+1}+\theta_{j-1}^{n+1}\right)+h\theta_j^{n+1}\\ &= \frac{h}{6}\delta^2\theta_j^{n+1}+h\theta_j^{n+1},\\ \int_\Omega \theta_h^{n}\psi_j\,dx &= \frac{h}{6}\delta^2\theta_j^{n}+h\theta_j^{n},\end{aligned}$$

where $\delta^2\theta_j^{n+1}=\theta_{j+1}^{n+1}-2\theta_j^{n+1}+\theta_{j-1}^{n+1}$.
We shall consider CFL numbers $\mu\in[0,1]$ and $v\le 0$, the case $v>0$ is handled by analogous argument. Then, the first term on the right side of (63) when it is approximate by vertex quadrature, depends on μ in the form

$$\begin{aligned}\int_\Omega (\theta_h^n(x-v\Delta t)-\theta_h^n(x))\psi_j(x)\,dx &= h\left((1-\mu)\theta_j^n+\mu\theta_{j+1}^n-\theta_j^n\right)\\ &= -h\mu\left(\theta_j^n-\theta_{j+1}^n\right).\end{aligned}$$

Hence, the scheme becomes, in operator notation

$$\frac{h}{6}\delta^2\theta_j^{n+1}+h\theta_j^{n+1}=-h\nu\left(\theta_j^n-\theta_{j+1}^n\right)+\frac{h}{6}\delta^2\theta_j^n+h\theta_j^n.$$

Replacing θ_j^n by $E^n e^{i\xi jh}$ gives

$$\left(1-\frac{2s^2}{3}\right)\lambda=-2\nu(s^2-isc)+1-\frac{2s^2}{3},$$

where $s=sin(\xi h/2)$ and $c=cos(\xi h/2)$, and λ is the amplification factor. For stability we require $|\lambda|^2\le 1$ for all $\xi\in[-\pi,\pi]$ which holds for $\mu\le 1/3$.

Acknowledgments

This research has been partially by Ministerio de Ciencia e Innovación (Spain) under research projects Consolider MATHEMATICA CSD2006-00032 and MTM2008- 02483.

References

[1] M. D. Baker, E. Süli, and A. F. Ware. Stability and convergence of the spectral Lagrange-Galerkin method for mixed periodic/non-periodic convection-dominated diffusion problems. *IMA J. Numer. Anal.*, 19:637–663, 1999.

[2] J. Baranger, D. Esslaoui, and A. Machmoum. Error estimate for convection problem with characteristics method. *Numer. Algorithms*, 21 (1999):49–56. Numerical methods for partial differential equations (Marrakech, 1998).

[3] J. Baranger and A. Machmoum. Une norme "naturelle" pour la méthode des caractéristiques en éléments finis discontinus: cas 1-D. *RAIRO Modél. Math. Anal. Numér.*, 30:549–574, 1996.

[4] J. Baranger and A. Machmoum. A "natural" norm for the method of characteristics using discontinuous finite elements: 2D and 3D case. *Math. Model. Numer. Anal.*, 33:1223–1240, 1999.

[5] M. Bause and P. Knabner. Uniform error analysis for Lagrange-Galerkin approximations of convection-dominated problems. *SIAM. J. Numer. Anal.*, 39:1954–1984, 2002.

[6] M. Bercovier, O. Pironneau, and V. Sastri. Finite elements and characteristics for some parabolic-hyperbolic problems. *Appl. Math. Modelling*, 7:89–96, 1983.

[7] A. Bermúdez and J. Durany. La methode des caracteristiques pour des problemes de convection-diffusion stationnaires. *M2AN. Math. Mod. and Num. Anal.*, 21:7–26, 1987.

[8] A. Bermúdez and J. Durany. Numerical solution of steady-state flow through a porous dam. *Comput. Methods Appl. Mech. Engrg.*, 68:55–65, 1988.

[9] A. Bermúdez. Continuum Thermomechanics. Birkhäuser Verlag, Berlin. *Progress in Mathematical Physics*, 43, 2005.

[10] A. Bermúdez, M. R. Nogueiras, and C. Vázquez. Numerical solution of (degenerated) convection-diffusion-reaction problems with higher order characteristics/finite elements. Part I: Time discretization. *SIAM. J. Numer. Anal.*, 44:1829–1853, 2006.

[11] A. Bermúdez, M. R. Nogueiras, and C. Vázquez. Numerical solution of (degenerated) convection-diffusion-reaction problems with higher order characteristics/finite elements. Part II: Fully Discretized Scheme and Quadrature Formulas. *SIAM. J. Numer. Anal.*, 44:1854–1876, 2006.

[12] K. Boukir, Y. Maday, B. Métivet, and E. Razafindrakoto. A high-order characteristics/finite element method for the incompressible Navier-Stokes equations. *Internat. J. Numer. Methods Fluids*, 25:1421–1454, 1997.

[13] D.R. Chenoweth and S. Paolucci. Natural convection in an enclosed vertical air layer with large horizontal temperature differences. *J. Fluid Mech.*, 169:173–210, 1986.

[14] G. de Vahl Davis. Natural convection of air in a square cavity: a benchmark numerical solution. *Internat. J. Numer. Methods Fluids*, 3:249–64, 1983.

[15] J. Douglas, Jr., C.-S. Huang, and F. Pereira. The modified method of characteristics with adjusted advection. *Numer. Math.*, 83:353–369, 1999.

[16] J. Douglas, Jr., and T.F. Russell. Numerical methods for convection-dominated difusion problems based on combining the method of characteristics with finite element or finite difference procedures. *SIAM J. Numer. Anal.*, 19:871–885, 1982.

[17] R.E. Ewing and T. F. Russel. Multistep galerkin methods along characteristics for convection-diffusion problems. *IMACS Publications. Advances in Computer Methods for Partial Differential Equations IV*, pages 28–36, 1981.

[18] G. Fourestey. Stabilité des méthodes de Lagrange-Galerkin du premier et du second ordre. *tech. report, INRIA, Raport de recherche*, 2002.

[19] L. D. Landau and E. M. Lifshitz. Fluid mechanics. Oxford. *Course of Theoretical Physics*, 6, 1982.

[20] M.T. Manzari. An explicit finite element algorithm for convective heat transfer problems. *Int. J. Numer. Meth. Heat Fluid Flow*, 9:860–877, 1999.

[21] N. Massarotti, P. Nithiarasu, and O.C. Zienkiewich. Characteristic-based-split (cbs) algorithm for incompressible flow problems with heat transfer. *Int. J. Numer. Meth. Heat Fluid Flow*, 8:969–990, 1998.

[22] K.W. Morton, A. Priestley, and E. Süli. Stability of the Lagrange-Galerkin Method with non-exac integration. *M2AN Math. Model. Numer. Anal.*, 22:625–653, 1988.

[23] C. Parés. éstude mathématique et approximation numérique de quelques ploblèmes aux limites de la mécanique des fluides incompressibles. Thèse. Université Paris VI. 1992.

[24] O. Pironneau. On the Transport-Diffusion Algorithm and Its Applications to the Navier-Stokes Equations. *Numer. Math.*, 38:309–332, 1982.

[25] O. Pironneau, J. Liou, and T. Tezduyar. Characteristic-Galerkin and Galerkin/least-squares space-time formulations for the advection-diffusion equations with time-dependent domains. *Comput. Methods Appl. Mech. Engrg.*, 100:117–141, 1992.

[26] A. Priestley. Exact projections and the Lagrange-Galerkin method: a realistic alternative to cuadrature. *J. Comput. Phys.*, 112:316–333, 1994.

[27] H. Rui and M. Tabata. A second order characteristic finite element scheme for convection-diffusion problems. *Numer. Math.*, 92:161–177, 2002.

[28] H. Schlichting and K. Gersten. Boundary layer theory. Ed. Springer-Verlag. 2004.

[29] E. Süli. Convergence and nonlinear stability of the Lagrange-Galerkin method for the Navier-Stokes equations. *Numer. Math.*, 53:459–483, 1988.

[30] E. Süli. Stability and convergence of the Lagrange-Galerkin method with non-exac integration.

Academic Press, London. *The mathematics of finite elements and applications, VI*, pages 435–442, 1988.

[31] E. Süli and A. Ware. A spectral mehod of characteristics for hyperbolic problems. *SIAM J. Numer. Anal.*, 28:423–445, 1991.

[32] M. Tabata and S. Fujima. Robustness of a characteristic finite element scheme of second order in time increment. *tech. report, MHF Preprint Series*, 2004.

[33] D. C. Wan, B. S. V. Patnaik, and G. W. Wei. A new Benchmark Quality Solution for the Buoyancy-Driven Cavity by Discrete Singular Convolution, Part B. *Numerical Heat Transfer*, 40:199–228, 2001.